Stability of Halo Orbits

J. E. Howard

Center for Integrated Plasma Studies, Campus Box 0390, University of Colorado, Boulder, Colorado 80309

H. R. Dullin

Department of Mathematical Sciences, Loughborough University, Loughborough, Leicestershire, LE11 3TU, United Kingdom

M. Horányi

Laboratory for Atmospheric and Space Physics and Department of Physics, Campus Box 0392, University of Colorado, Boulder, Colorado 80309

We predict new populations of trapped nonequatorial ("halo") orbits of charged dust grains about an arbitrary axisymmetric planet. Simple equilibrium and stability conditions are derived, revealing dramatic differences between positively and negatively charged grains in prograde or retrograde orbits. Implications for the Cassini mission to Saturn are discussed.

With the Cassini spacecraft on route to Saturn to perform detailed *in situ* measurements of charged dust grains, it is important to understand the nonlinear dynamics of their orbital motion [1–7]. We report here a complete equilibrium and stability analysis for charged dust grains of arbitrary position and velocity about an axisymmetric planet. The results yield quantitative predictions concerning the possible size and charge of dust grains reaching the Cosmic Dust Analyzer (CDA) [8] aboard the Cassini Orbiter. Stable halo orbits (those encircling the planet above or below the equatorial plane) are found to be of three types: positively charged grains in prograde orbits at large orbital radius, retrograde orbits at any radius, and prograde negatively charged grains at very high latitudes. The results suggest that positively charged grains in retrograde orbits are the most likely to be observed by the CDA.

Our physical model and methodology closely parallel those employed by Howard *et al.* [9]: Keplerian gravity, corotating magnetic field (taken to be an aligned centered dipole), and induced electric field. Planetary oblateness, radiation pressure, and plasma drag are neglected. As we shall see, the mixture of gravitational and electromagnetic forces generates a very rich dynamical behavior, which will be reported in detail elsewhere [10]. Equilibria are found as the critical points of an effective potential U^e, with local nonlinear (Lyapunov) stability boundaries given by $\det D^2 U^e = 0$. The critical points are given by the zeros of a quintic polynomial in the radial coordinate r, whose double zeros correspond to the zeros of $\det D^2 U^e$, leading to surprisingly simple explicit stability boundaries.

For a spherical dust grain of uniform density ρ_m (g/cm^3), radius a_μ (microns), and a surface potential of Φ (volts),

$$\frac{q}{m} = \frac{10^6 \Phi}{4\pi \rho_m a_\mu^2} \text{ esu/g}. \quad (1)$$

We shall take $\rho_m = 1$ g/cm^3. Typical values of Φ for Jupiter and Saturn lie in the range -20 V $< \Phi < +10$ V [11]. For a given planet and equilibrium radial position r, stability depends on q/m alone, conveniently measured by the parameter $\hat\Phi = \Phi/a_\mu^2$, which we shall express as a pure number. Since the potential is determined by the ambient plasma, $\hat\Phi$ depends only on the grain radius a_μ. An upper bound on $\hat\Phi$ is thus a lower bound on a_μ. Roughly speaking, grains with $a_\mu > 1$ are gravity dominated, while those with $a_\mu < 1$ are dominated by electromagnetic forces.

Equilibria.—Consider a dust grain of mass m and charge q orbiting about an axisymmetric planet. As in [9] the motion may be described in an inertial frame by an effective potential, in Gaussian units and cylindrical coordinates,

$$U^e = \frac{1}{2m\rho^2}\left(p_\phi - \frac{q\Psi}{c}\right)^2 + U + \frac{q\Omega}{c}\Psi, \quad (2)$$

where $U(\rho, z)$ is the gravitational potential, $\Psi(\rho, z)$ is the magnetic stream function, $p_\phi = m\rho^2\omega + q\Psi/c$ is the conserved canonical momentum, ω is the orbital frequency, and Ω is the planetary rotation rate. Here we assume Keplerian gravity, $U = -\mu m/r$, with $\mu = GM_s$, $r = \sqrt{\rho^2 + z^2}$, and a centered dipole field, for which $\Psi = \gamma \rho^2/r^3$, where $\gamma = qB_0 R_p^3/c$ measures the dipole strength, with B_0 the magnetic field on the planetary equator. Measuring distances in units of the planetary radius, R_p, (2) becomes

$$U^e = \frac{1}{2\rho^2}\left(p_\phi - \frac{\omega_c \rho^2}{r^3}\right)^2 - \frac{\omega_k^2}{r} + \frac{\Omega\omega_c\rho^2}{r^3}, \quad (3)$$

where $\omega_c = qB_0/mc$ is the cyclotron frequency and $\omega_k = \sqrt{\mu/R_p^3}$ is the Kepler frequency, both evaluated *on the planetary equator*, and now $p_\phi = \rho^2\omega + \omega_c\rho^2/r^3$.

Equilibria (ρ_0, z_0) are given by the simultaneous solutions of $U_\rho^e = U_z^e = 0$, which for $z_0 \neq 0$ reduce to

$$r^5\omega^2 + \omega_c(\omega - \Omega)(2r^2 - 3\rho^2) = \omega_k^2 r^2, \quad (4)$$

$$3\omega_c(\omega - \Omega)\rho^2 + \omega_k^2 r^2 = 0, \quad (5)$$

where p_ϕ has been eliminated in favor of ω. It follows immediately from (5) that the orbital frequency $\omega \neq \Omega$, i.e., *nonequatorial synchronous orbits are impossible.* Furthermore, we see that it is necessary that $\omega < \Omega$ for positive charge and $\omega > \Omega$ for negative charge. Note that the latter inequalities also hold for equatorial orbits [9]; the new fact of life is that *exact* synchronicity is unattainable for nonequatorial orbits.

First suppose it is desired to know whether a stable equilibrium orbit exists for some $\hat{\Phi}$ (and therefore ω_c) at a specified location (ρ_0, z_0). Eliminating ω_c between (4) and (5) gives

$$\omega^2 = \frac{2\omega_k^2}{3\rho_0^2 r_0}. \quad (6)$$

Both signs of ω are possible. The requisite value of $\hat{\Phi}(\omega_c)$ (if it exists) is then given by

$$\omega_c = \frac{r_0^3 \omega^2}{2(\Omega - \omega)}. \quad (7)$$

For positive charge this is automatically satisfied for negative (retrograde) ω but demands $\omega < \Omega$ for positive (prograde) ω. For negative charge we need $\omega > \Omega > 0$, which excludes retrograde orbits. There are no retrograde nonequatorial equilibria for negative charge; for positive charge either sense is possible.

Now (7) can be written as a quadratic in ω, similar to that previously found for equatorial orbits:

$$r_0^3 \omega^2 + 2\omega_c(\omega - \Omega) = 0. \quad (8)$$

Thus, we can take the point of view that r_0 and ω_c are specified and seek conditions for an equilibrium somewhere on the sphere $r = r_0$. The solutions of (8) are

$$r_0^3 \omega = -\omega_c \pm \sqrt{\omega_c^2 + 2r_0^3 \Omega \omega_c} \quad (9)$$

subject to the constraint $\rho < r$. Equation (6) then implies $\omega^2 \geq \omega^{*2} = 2\omega_k^2/3r_0^3$, with corresponding ω_c given by (7), which yields $(\omega^* > 0)$

$$\omega_k^2/3(\Omega + \omega^*) \leq \omega_c \leq \omega_k^2/3(\Omega - \omega^*). \quad (10)$$

Figure 1 shows these solutions for $r_0 = 2$. For $\omega_c > 0$ and $|\omega| > \omega^*$ there is a prograde/retrograde pair; for $-2r_0^3\Omega < \omega_c < 0$ there are no equilibria, and for $\omega_c < -2r_0^3\Omega$ there are two possible prograde equilibria. Since $\omega^* < \Omega$ there are no constraints on q/m. For large q/m there are two asymptotic limits: $\omega \approx \Omega$ and $\omega \approx -\Omega - 2\omega_c/r_0^3$.

Stability.—In general an equilibrium (ρ_0, z_0) is Lyapunov stable if both $\det D^2 U^e > 0$ and $\mathrm{tr} D^2 U^e > 0$ [12], with stability boundaries given by $\det D^2 U^e = 0$. Just as for the equatorial equilibria we can generate a stability

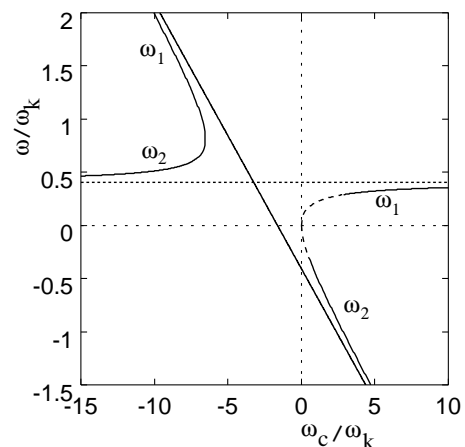FIG. 1.   Orbital frequencies $\omega_{1,2}$ as functions of ω_c/ω_k for $r_0 = 2.0$. Equilibria do not exist on the dashed part of the right-hand curve ($q > 0$).

diagram with r_0/R_p plotted vs ω_c/ω_k. The corresponding values of ρ_0 and z_0 (if they exist) then follow from (6). As a preliminary step, let us reduce the number of parameters by rescaling $\hat{r} = r/\lambda$, $\hat{\rho} = \rho/\lambda$, with scale length $\lambda = p_\phi/\gamma$, which gives

$$U^e = \frac{\alpha}{2\hat{\rho}^2}\left(1 - \frac{\hat{\rho}^2}{\hat{r}^3}\right)^2 - \frac{1}{\hat{r}} + \frac{\delta\hat{\rho}^2}{\hat{r}^3}, \quad (11)$$

where we have introduced the dimensionless parameters $\alpha = p_\phi^3/\mu m^2\gamma$ and $\delta = \gamma\Omega/\mu m$. The equilibrium conditions may then be reduced to the quintic

$$P_5(\tilde{r}) = 2\tilde{r}^5 - 9\beta\tilde{r}^4 + 12\beta\tilde{r}^3 + \beta\tilde{r}^2 + 6\beta^2 = 0, \quad (12)$$

where $\beta = \alpha\delta^2$, $\tilde{r} = \hat{r}/\delta$, and the corresponding ρ value is given by

$$\hat{\rho}^2 = \frac{\delta^3(3\beta + \tilde{r}^2)\tilde{r}^3}{3(\beta + \tilde{r}^3)}. \quad (13)$$

In general the quintic (12) has two positive real roots. In order that one of these roots be physically realized it must satisfy the constraint $\hat{\rho} < \hat{r}$.

Now observe that an instability invariably involves the merging of two zeros of $P_5(\tilde{r})$. That is, $P_5(\tilde{r})$ has a double zero whenever $\det D^2 U^e = 0$. Setting the discriminant of $P_5(\tilde{r})$ to zero yields $\beta^* = 5/8 + 13\sqrt{3}/36 = 1.250\,463$, at which point $\tilde{r}^* = 3/2 + 5\sqrt{3}/6 = 2.943\,38$. From the scale length

$$\lambda = \frac{\gamma}{p_\phi} = \frac{\omega_c R_p}{\rho_0^2(\omega + \omega_c/r_0^3)} \quad (14)$$

it follows that

$$\tilde{r}^* = \frac{2\Omega}{3\omega^2}(\omega + \omega_c/r_0^3). \quad (15)$$

Eliminating ω between (15) and the quadratic (8) then gives

$$r_0 = (A\omega_c/\Omega)^{1/3}, \quad (16)$$
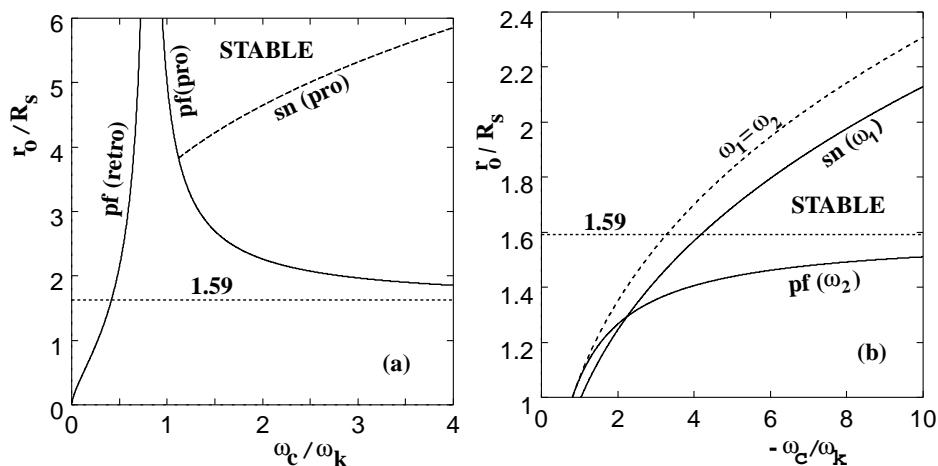
3245

FIG. 2. Stability diagram for (a) positive charge, (b) negative charge. For positive charge, prograde orbits are stable in the upper triangular region; retrograde orbits are stable everywhere to the right of the curve labeled pf(retro). For negative charge only prograde orbits can be stable. Equilibrium orbits appear on the curve $\omega_1 = \omega_2$, stabilizing (for $r_0 > 1.3R_s$) upon crossing the curve labeled sn(ω_1).

where $A = 2(5 + 3\sqrt{3})$, with corresponding orbital frequency $\omega = (2 - \sqrt{3})\Omega$.

Figure 2(a) presents the stability boundaries in the $\omega_c/\omega_k - r_0$ plane. For the prograde branch halo orbits are born on the curve marked pf(pro), where an equatorial orbit suffers a pitchfork bifurcation. Note that this boundary has a vertical asymptote when $\delta = 1/3$. For $r_0 > 3.83R_s$ this orbit is stable until it reaches the curve labeled sn(pro), where it undergoes a saddle-node bifurcation ($\beta = \beta^*$); for $r_0 < 3.83R_s$ all equilibria are unstable. A representative stable equilibrium is illustrated in Fig. 3(a), which depicts level sets of U^e for $r_0 = 5$ and $\hat{\Phi} = 1200$. In this case a rather complex set of global bifurcations (reconnections) occur as $\hat{\Phi}$ is varied. The planetary surface is drawn in as a circle of unit radius. For the retrograde branch the behavior is much simpler. Here halo orbits are born out of an equatorial pitchfork bifurcation [curve pf(retro)] for all r_0 and remain stable

ever after, i.e., nothing happens to them with increasing $\hat{\Phi}$. A typical stable equilibrium for a point near the Cassini Division, $r_0 = 2$ and $\hat{\Phi} = 800$, is depicted in Fig. 3(b). As shown in [9], the equatorial stability boundaries (solid curves) are given by the two branches of

$$\rho_0 = \frac{(6\omega_c^2)^{1/3}}{(\omega_k^2 - 3\Omega\omega_c)^{2/3}}. \qquad (17)$$

For negatively charged grains a similar analysis yields the stability diagram shown in Fig. 2(b). Both modes appear as unstable saddles on the same curve, given by the vanishing of the determinant of the quadratic (8):

$$r_0 = (\omega_c/2\Omega)^{1/3}. \qquad (18)$$

On this curve $\omega_1 = \omega_2 = \omega_c/r_0^3$, the local equatorial cyclotron frequency. Equilibria are given by a quintic similar to (12), which has a double zero at $\tilde{r}^* = 3/2 - 5\sqrt{3}/6$ for $\beta = 5/8 - 13\sqrt{3}/36$. The resulting stability boundary is,
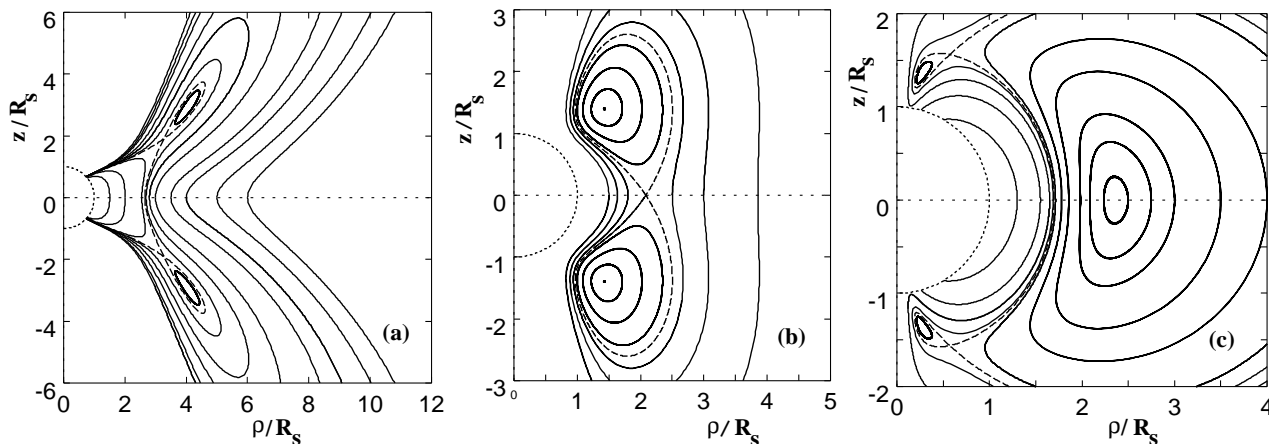

FIG. 3. Selected level sets of U^e for (a) prograde positive charge, with $r_0 = 5$ and $\hat{\Phi} = 1200$; (b) retrograde positive charge, with $r_0 = 2$ and $\hat{\Phi} = 800$; and (c) prograde negative charge, with $r_0 = 1.381$ and $\hat{\Phi} = 3000$.
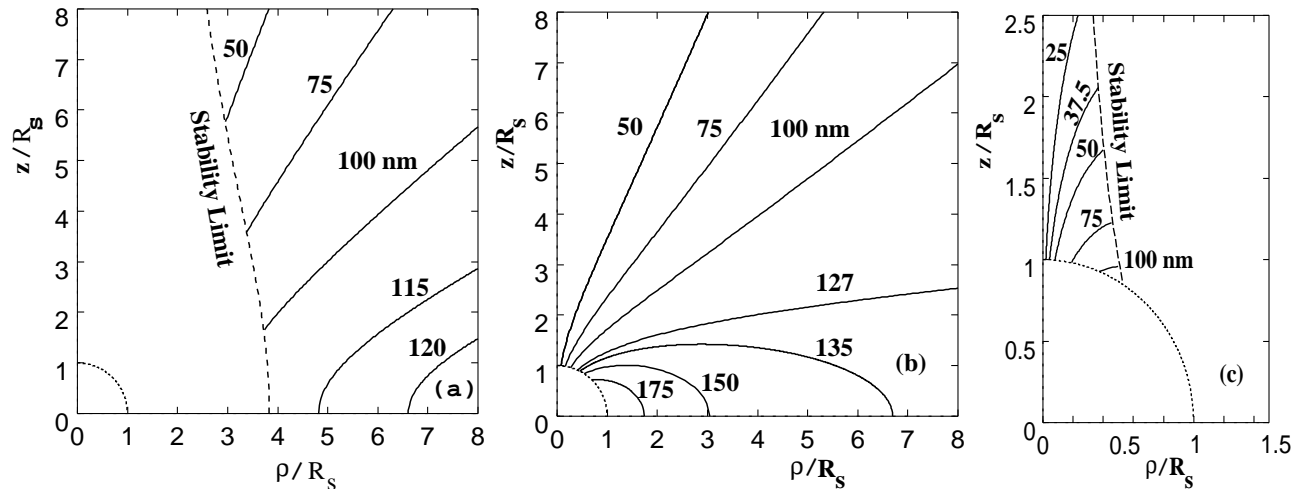
FIG. 4. Loci of stable equilibria for stable halo orbits about Saturn for several grain radii and (a) prograde positive charge, (b) retrograde positive charge, and (c) prograde negative charge.

for $\omega = \omega_1$,

$$r_0 = (B\omega_c/\Omega)^{1/3}, \qquad (19)$$

where $B = 2(3\sqrt{3} - 5)$, on which $\omega = (2 + \sqrt{3})\Omega$, and labeled $\mathrm{sn}(\omega_1)$ in Fig. 2(b). An unstable equilibrium orbit appears on the $\omega_1 = \omega_2$ curve, stabilizing upon crossing the $\mathrm{sn}(\omega_1)$ boundary. The second mode ($\omega = \omega_2$) remains unstable, disappearing into the equatorial plane upon reaching the curve labeled $\mathrm{pf}(\omega_2)$. Figure 3(c) shows level sets of U^e for $r_0 = 1.381$ and $\hat{\Phi} = 3000$. In this case the small nonequatorial wells coexist with a large equatorial well extending to large latitude.

These results have important implications for the Cassini mission. For fixed plasma potential it is easy to locate halo orbits of a given grain size. Taking $\Phi = 10$ V gives the loci of stable equilibria shown in Fig. 4(a) for a positively charged grain in a prograde orbit about Saturn. This was done by treating r_0 as parameter, solving (8) for ω and getting ρ_0 from (6). The dashed curve corresponds to the inner stability boundary (18) and has the form $\rho^2 r = $ const. The maximum possible stable grain radius for this value of Φ is 128 nm.

Figure 4 presents quantitative predictions of what might be observed by the CDA. For example, Fig. 4(a) shows that there are no stable positive prograde halo orbits whatsoever within a spherical radius of $r = 3.83R_s$, with only very small grains penetrating to higher latitudes. Such small grains in prograde orbits are unlikely to be detected by the CDA. Positive grains in retrograde halo orbits, on the other hand, are stable for all radii, as shown in Fig. 4(b). The high relative velocities of these grains with respect to the Cassini Orbiter make them easy to detect by the CDA. Note that in this case [see Fig. 3(b)] there are two topologically distinct families of trapped orbits, those which cross the equatorial plane and true halo orbits trapped near a nonequatorial equilibrium. These two classes have similar energies and could equally well reach

the CDA at a nonequatorial position. However, whether reflecting particles survive repeated midplane crossings depends on equatorial radius; generally grains outside the main rings ($\rho_0 \gtrsim 2.3R_s$) have the best chance of surviving. Finally, Fig. 4(c) presents loci of stable equilibria for prograde negatively charged grains. In contrast to prograde positive charge, negative halo orbits are seen to be restricted to very small grains at very high latitudes. In conclusion, it appears that the most likely candidates for CDA-detectable orbits are to be found among the retrograde positively charged grains.

[1] E. Grün, G. E. Morfill, and D. A. Mendis, in *Planetary Rings*, edited by R. Greenberg and A. Brahic (University of Arizona Press, Tuscon, 1984).

[2] D. A. Mendis, J. R. Hill, W.-H. Ip, C. K. Goertz, and E. Grün, in *Saturn*, edited by T. Gehrels and M. Matthews (University of Arizona Press, Tuscon, 1984).

[3] R.-L. Xu and L. F. Houpis, J. Geophys. Res. **90**, 1375 (1985).

[4] L. Schaffer and J. A. Burns, J. Geophys. Res. **100**, 213 (1995).

[5] D. F. Hamilton, Icarus **101**, 244 (1993).

[6] T. G. Northrop and J. R. Hill, J. Geophys. Res. **87**, 6045 (1982).

[7] D. A. Mendis, J. R. Hill, and H. L. F. Houpis, J. Geophys. Res. **88**, A929 (1983).

[8] R. Srama *et al.* (to be published).

[9] J. E. Howard, M. Horányi, and G. R. Stewart, Phys. Rev. Lett. **83**, 3993 (1999).

[10] H. R. Dullin, J. E. Howard, M. Horányi, and G. A. Stewart (to be published).

[11] M. Horányi, Annu. Rev. Astron. Astrophys. **34**, 383 (1966).

[12] V. I. Arnold, *Mathematical Methods of Classical Mechanics* (Springer, New York, 1978), 2nd ed.